

Production of $t\bar{t}b\bar{b}$ at the LHC at NLO QCD *

A. Bredenstein^a, A. Denner^b, S. Dittmaier^c and S. Pozzorini^d

^aHigh Energy Accelerator Research Organization (KEK), Tsukuba, Ibaraki 305-0801, Japan

^bPaul Scherrer Institut, Würenlingen und Villigen, CH-5232 Villigen PSI, Switzerland

^cAlbert-Ludwigs-Universität Freiburg, Physikalisches Institut, D-79104 Freiburg, Germany

^dPhysics Department, Theory Group, CERN, CH-1211 Geneva 23, Switzerland

We summarise predictions for $t\bar{t}b\bar{b}$ production at the LHC in next-to-leading order QCD. The precise description of this background process is a prerequisite to observe associated $t\bar{t}H$ production in the $H \rightarrow b\bar{b}$ decay channel. The one-loop amplitudes are computed using Feynman diagrams and numerical tensor reduction. This approach provides very high numerical stability and CPU efficiency. We find that the scale choice adopted in ATLAS simulations underestimates the $t\bar{t}b\bar{b}$ background by a factor two and introduce a new dynamical scale that stabilises the perturbative predictions. In the regime of highly boosted Higgs bosons, which offers better perspectives to observe the $t\bar{t}H(H \rightarrow b\bar{b})$ signal, the corrections induce significant distortions in the kinematic distributions.

1. Introduction

The discovery of the Higgs boson and the measurement of its interactions with massive quarks and vector bosons represent a central goal of the Large Hadron Collider (LHC). For a light Higgs boson, $M_H \lesssim 130$ GeV, associated $t\bar{t}H$ production provides the opportunity to observe the Higgs boson in the $H \rightarrow b\bar{b}$ decay channel and to measure the top-quark Yukawa coupling. However, the extraction of the $t\bar{t}H(H \rightarrow b\bar{b})$ signal from its large QCD backgrounds, $pp \rightarrow t\bar{t}b\bar{b}$ and $t\bar{t}jj$, represents a serious challenge. The selection strategies elaborated by ATLAS and CMS [1,2] anticipate a statistical significance around 2σ and a signal-to-background ratio as low as 1/10. This calls for better than 10% precision in the background description, a very demanding requirement both from the experimental and theoretical point of view. Very recently, a novel selection strategy based on highly boosted Higgs bosons has opened new and very promising perspectives [3]. This ap-

proach might increase the signal-to-background ratio beyond 1/3. Moreover, three b-taggings would be sufficient to strongly suppress the $t\bar{t}jj$ contamination so that the background would be completely dominated by $t\bar{t}b\bar{b}$ production.

The calculation of the next-to-leading-order (NLO) QCD corrections to the irreducible $t\bar{t}b\bar{b}$ background, first presented in Refs. [4,5,6] and subsequently confirmed in Ref. [7], constitutes another important step towards the observability of $t\bar{t}H(H \rightarrow b\bar{b})$ at the LHC. These NLO predictions are mandatory in order to reduce the huge scale uncertainty of the lowest-order (LO) $t\bar{t}b\bar{b}$ cross section, which can vary up to a factor four if the QCD scales are identified with different kinematic parameters [8]. Motivated by results for the signal process $pp \rightarrow t\bar{t}H$ [9], where a moderate K factor ($K \simeq 1.2$) had been found [9], experimental groups adopted the scale $\mu_{R,F} = m_t + m_{b\bar{b}}/2$ for the LO simulation of the $t\bar{t}b\bar{b}$ background [1]. However, at this scale the NLO corrections to $pp \rightarrow t\bar{t}b\bar{b}$ turn out to be large ($K \simeq 1.8$) [5,7].

The calculation of the NLO corrections to $pp \rightarrow t\bar{t}b\bar{b}$ constitutes also an important technical benchmark. The description of many-particle processes at NLO plays a central role for the LHC

*This work is supported in part by the European Community's Marie-Curie Research Training Network under contract MRTN-CT-2006-035505 "Tools and Precision Calculations for Physics Discoveries at Colliders" and the Japan Society for the Promotion of Science.

physics programme, and the technical challenges raised by these calculations have triggered an impressive amount of conceptual and technical developments. Within the last year, this progress has led to the first NLO results for six-particle processes at the LHC, namely for $pp \rightarrow t\bar{t}b\bar{b}$ [5,7], $pp \rightarrow t\bar{t}jj$ [10], the leading- [11] and the full-colour contributions [12] to $pp \rightarrow Wjjj$, for $pp \rightarrow Z/\gamma jjj$ [13] and for the $q\bar{q}$ contribution to $pp \rightarrow b\bar{b}b\bar{b}$ [14].

To compute the virtual corrections to $t\bar{t}b\bar{b}$ production we employ explicit Feynman-diagrammatic representations of the one-loop amplitudes and numerical reduction of tensor integrals [15]. The factorisation of colour matrices, the algebraic reduction of helicity structures, and the systematic recycling of a multitude of common subexpressions—both inside individual diagrams and in tensor integrals of different diagrams that share common sub-topologies—strongly mitigate the factorial complexity that is inherent in Feynman diagrams and lead to a remarkably high CPU efficiency. Our results have been confirmed with the HELAC-1LOOP implementation of the OPP method [16,17,18] within the statistical Monte Carlo error of 0.2% [7].

2. Outline of the calculation

In LO, the hadronic production of $t\bar{t}b\bar{b}$ proceeds via the partonic processes $q\bar{q} \rightarrow t\bar{t}b\bar{b}$ and $gg \rightarrow t\bar{t}b\bar{b}$, which are described by 7 and 36 tree diagrams, respectively. The corresponding virtual NLO QCD corrections involve 188 and 1003 one-loop diagrams. The real emission contributions comprise the crossing-symmetric channels $q\bar{q} \rightarrow t\bar{t}b\bar{b}g$, $qg \rightarrow t\bar{t}b\bar{b}q$, and $g\bar{q} \rightarrow t\bar{t}b\bar{b}q$, which involve 64 tree diagrams each, and the channel $gg \rightarrow t\bar{t}b\bar{b}g$ with 341 diagrams. Each of these contributions has been worked out twice and independently, resulting in two completely independent computer codes.

The virtual corrections are calculated in the Feynman-diagrammatic approach. The diagrams are generated with two independent versions of FEYNARTS [19,20] and algebraically simplified with two in-house MATHEMATICA programs that generate FORTRAN77 code in a fully automatised

way. One of the two programs relies on FORM-CALC 5.2 [21] for preliminary algebraic manipulations. The virtual corrections are obtained from the interference of the one-loop and LO matrix elements on a diagram-by-diagram basis.

Owing to colour factorisation for individual (sub)diagrams colour sums can be performed very efficiently. The colour-summed result is given by a combination of previously computed colour-Born interference terms. This requires a *single evaluation* of the non-trivial colour-stripped amplitude of each (sub)diagram.

Helicity structures are handled in a similar way. The helicity-dependent parts of all diagrams are reduced to a common basis of so-called Standard Matrix Elements (SMEs), and helicity sums are performed once and for all at the level of the SMEs-Born interference. The diagram-independent treatment of the helicity-dependent parts of loop graphs is made possible by the covariant decomposition of tensor integrals.

The one-loop amplitudes are expressed as linear combinations of tensor-integral coefficients. The latter are evaluated by two independent *numerical* FORTRAN libraries that recursively reduce them to master integrals using the methods of Ref. [15]. Avoiding an explicit reduction of analytic expressions to master integrals, this numerical approach prevents prohibitively large expressions and permits to adapt the reduction strategy to the specific numerical problems that appear in different phase-space regions. An automatic cache system is implemented that strongly boosts the reduction by recycling a multitude of tensor integrals among Feynman diagrams with common sub-topologies.

Ultraviolet (UV) divergences are regularized dimensionally throughout, but infrared (IR) divergences are treated in different variants, which comprise pure dimensional regularization with strictly massless light quarks and a hybrid scheme with small quark masses. The corresponding scalar integrals are evaluated using the methods and results of Ref. [22,23], and different regularization schemes are translated into each other as described in Ref. [24].

The treatment of rational parts is greatly simplified by the fact that rational terms result-

ing from $1/\epsilon$ and $1/\epsilon^2$ poles of IR kind vanish in truncated one-loop amplitudes [4]. Rational terms arising from UV poles of tensor integrals with D -dependent coefficients are automatically extracted by means of a catalogue of residues.

The reduction to SMEs is performed in such a way that no spurious poles are generated that might cause numerical instabilities. It starts with process-independent D -dimensional relations such as momentum conservation, Dirac algebra, transversality, and gauge-fixing conditions for the gluon-polarisation vectors. Once rational terms are extracted, we further reduce SMEs with two alternative algorithms in four dimensions. For the gluon induced process, the first algorithm splits each fermion chain into two contributions, $u(p_i) = \sum_{\lambda=\pm} \omega_\lambda u(p_i)$, via insertion of chiral projectors $\omega_\pm = (1 \pm \gamma^5)/2$. This permits to employ various relations of type $\gamma^\mu \gamma^\alpha \gamma^\beta \omega_\pm \otimes \gamma_\mu = \gamma^\mu \omega_\pm \otimes (\gamma_\mu \gamma^\beta \gamma^\alpha \omega_\pm + \gamma^\alpha \gamma^\beta \gamma_\mu \omega_\mp)$, which connect Dirac matrices of different fermion chains [4,25], to reduce the full amplitude to 502 SMEs [6]. Besides this procedure, which depends on process-specific aspects, we implemented a simple process-independent reduction based on a single four-dimensional identity of type $\gamma^{\mu_1} \gamma^{\mu_2} \gamma^{\mu_3} \gamma^{\mu_4} \gamma^{\mu_5} = g^{\mu_1 \mu_2} \gamma^{\mu_3} \gamma^{\mu_4} \gamma^{\mu_5} - g^{\mu_1 \mu_2} g^{\mu_3 \mu_4} \gamma^{\mu_5} + \text{perm.}$, which eliminates spinor chains with more than three Dirac matrices without introducing γ_5 [6]. This leads to 970 SMEs. In spite of the factor-two difference in the number of SMEs, the numerical codes based on the two different reductions have the same—and remarkably high—CPU speed: about 180 ms per phase-space point. Thus, the obtained CPU performance, at least for this process, does not depend on process-dependent optimisations.

To handle singularities in the real corrections we employed the dipole subtraction method [26], in particular the MADDIPOLE implementation [27] in one of our calculations. The $2 \rightarrow 5$ matrix elements were generated with MADGRAPH [28] and checked against analytic calculations with the Weyl–van der Waerden spinor formalism and in-house code based on off-shell recursions. More details are given in Ref. [6].

3. Predictions for the LHC

We study the process $pp \rightarrow t\bar{t}b\bar{b} + X$ at $\sqrt{s} = 14$ TeV with $m_t = 172.6$ GeV and massless b quarks. Massless final-state partons with rapidity–azimuthal-angle separation $\sqrt{\Delta\phi^2 + \Delta y^2} < D = 0.4$ are recombined into jets using a k_T -algorithm, and we require two b jets with $p_{T,b} > 20$ GeV and $|y_b| < 2.5$. We use the CTEQ6 set of PDFs but neglect the suppressed contributions from b quarks in the initial state. More details are given in Ref. [6].

In all recent ATLAS studies of $t\bar{t}H(H \rightarrow b\bar{b})$ [1,8,29] the signal and its $t\bar{t}b\bar{b}$ background were simulated by setting the renormalisation and factorisation scales equal to half the threshold energy, $E_{\text{thr}} = 2m_t + m_{b\bar{b}}$. In Ref. [5] we found that for this scale choice the NLO corrections to $pp \rightarrow t\bar{t}b\bar{b}$ are close to a factor of two. This enhancement is due to the fact that $pp \rightarrow t\bar{t}b\bar{b}$ is a multi-scale process involving various scales well below $E_{\text{thr}}/2$. The inspection of differential distributions reveals that the cross section is saturated by b quarks with $p_{T,b} \ll m_t$. Therefore we introduced in Ref. [6] the dynamical scale

$$\mu_0^2 = m_t \sqrt{p_{T,b} p_{T,\bar{b}}}, \quad (1)$$

which improves the perturbative convergence and minimises NLO effects in the shape of distributions.

Using the scale (1), we discussed in Ref. [6] the kinematic region $m_{b\bar{b}} > 100$ GeV and found that for all distributions considered the NLO corrections are at the level of 20–30% and have relatively little impact on the shape of distributions. On the other hand we the corrections still induce significant distortions of the kinematic distributions in the regime of a highly boosted Higgs boson, which offers better perspectives to observe the $t\bar{t}H$ signal. Here we provide some distributions in this scenario with $p_{T,b\bar{b}} > 200$ GeV.

In Figure 1 we show the scale dependence of the LO and NLO integrated cross sections. Renormalisation (μ_R) and factorisation (μ_F) scales are varied around the central value (1),

$$\mu_R = \xi_R \mu_0, \quad \mu_F = \xi_F \mu_0. \quad (2)$$

in a uniform ($\xi_F = \xi_R$) and antipodal ($\xi_F = \xi_R^{-1}$) way in the range $1/8 \leq \xi_F, \xi_R \leq 8$. At the

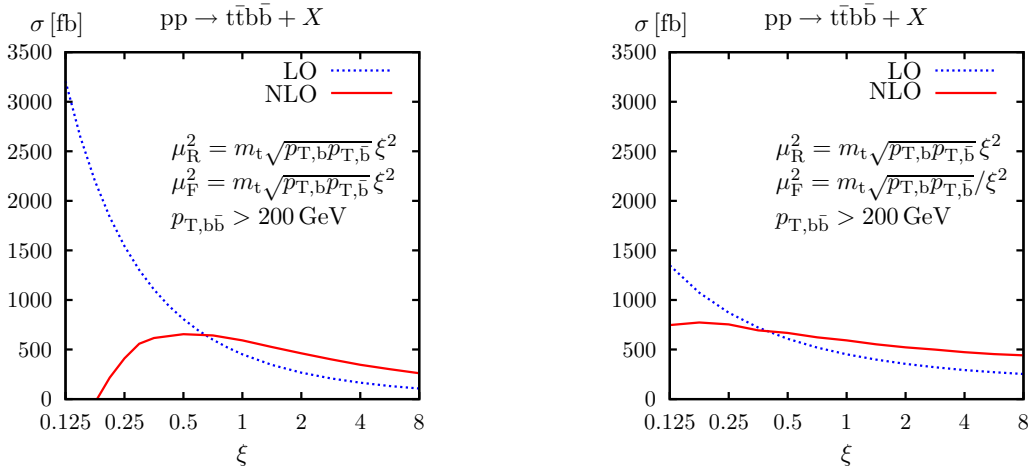


Figure 1. Scale dependence of the LO and NLO $pp \rightarrow t\bar{t}b\bar{b} + X$ cross section. The left and the right plots describe uniform ($\xi_R = \xi_F = \xi$) and antipodal ($\xi_R = \xi_F^{-1} = \xi$) scale variations, respectively.

central scale we obtain $\sigma_{\text{LO}} = 451.8(2)$ fb and $\sigma_{\text{NLO}} = 592(4)$ fb corresponding to $K = 1.31$. The shape of the scale-dependence curves indicates good convergence and stability of the perturbative expansion. The shifts induced by factor-two variations of the QCD scales amount to 79% in LO and 22% in NLO.

For distributions we provide LO and NLO predictions with uncertainty bands for factor-two uniform scale variations, which have a larger impact as antipodal variations. More precisely, all observables are evaluated at three different scales: $\xi_F = \xi_R = 0.5, 1, 2$.

The $b\bar{b}$ invariant-mass distribution is displayed in Figure 2. The NLO corrections induce an appreciable shape distortion of about 20%, in particular near the physically interesting region of $m_{b\bar{b}} \sim 100$ GeV. Such an effect tends to mimic a Higgs signal and should be carefully taken into account in the $t\bar{t}H(H \rightarrow b\bar{b})$ analysis.

For other distributions the shape distortion is not as sizeable. As examples we show the distribution in the azimuthal angle $\phi_{b\bar{b}}$ that represents the azimuthal orientation of the b jets with respect to the beam direction in the plane perpendicular to the $b\bar{b}$ momentum in Figure 3 and the dependence of the cross section with respect to a cut on the $t\bar{t}b\bar{b}$ invariant mass in Figure 4.

4. Conclusion

The observation of the $t\bar{t}H(H \rightarrow b\bar{b})$ signal at the LHC requires a very precise description of the $t\bar{t}b\bar{b}$ irreducible background. The NLO QCD corrections reveal that the scale choice adopted in previous LO simulations of $pp \rightarrow t\bar{t}b\bar{b}$ does not account for the multi-scale character of this process and underestimates its cross section by a factor of two. A suitably chosen dynamical scale significantly reduces both the K factor and the residual NLO scale uncertainty. For standard cuts NLO effects feature a relatively small kinematic dependence, but in the regime of highly boosted Higgs bosons significant distortions are still present in the shape of some distributions.

REFERENCES

1. G. Aad *et al.* [The ATLAS Collaboration], arXiv:0901.0512 [hep-ex].
2. G. L. Bayatian *et al.* [CMS Collaboration], J. Phys. G **34** (2007) 995.
3. T. Plehn, G. P. Salam and M. Spannowsky, Phys. Rev. Lett. **104**, 111801 (2010) [arXiv:0910.5472 [hep-ph]].
4. A. Bredenstein, A. Denner, S. Dittmaier and S. Pozzorini, JHEP **0808** (2008) 108 [arXiv:0807.1248 [hep-ph]].

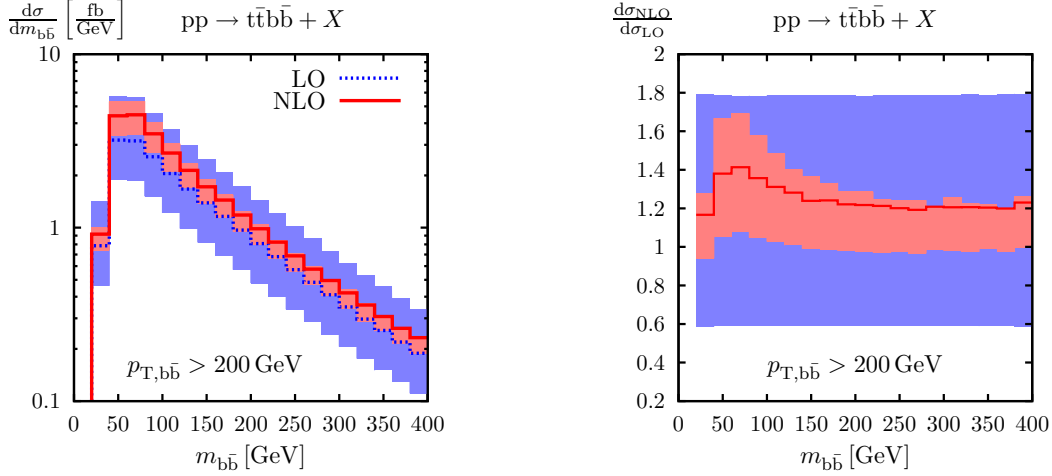


Figure 2. Invariant-mass distribution of the $b\bar{b}$ pair: absolute LO and NLO predictions (left) and NLO K factor (right).

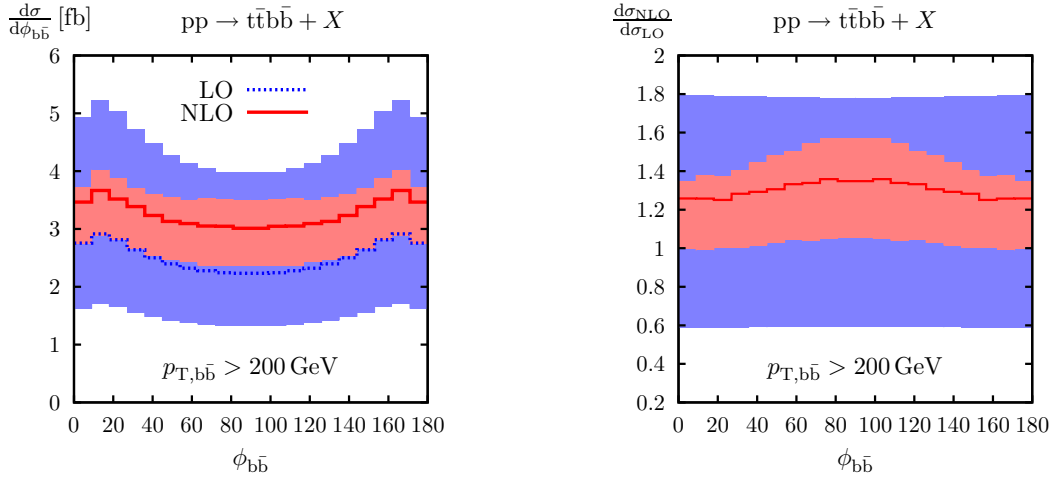


Figure 3. Azimuthal orientation of the b jets in the plane perpendicular to the $b\bar{b}$ system: absolute LO and NLO predictions (left) and NLO K factor (right).

5. A. Bredenstein, A. Denner, S. Dittmaier and S. Pozzorini, Phys. Rev. Lett. **103** (2009) 012002 [arXiv:0905.0110 [hep-ph]].
6. A. Bredenstein, A. Denner, S. Dittmaier and S. Pozzorini, JHEP **1003** (2010) 021 [arXiv:1001.4006 [hep-ph]].
7. G. Bevilacqua *et al.*, JHEP **0909** (2009) 109 [arXiv:0907.4723 [hep-ph]].
8. B. P. Kersevan and E. Richter-Was, Eur. Phys. J. C **25** (2002) 379 [arXiv:hep-ph/0203148]; Comput. Phys. Commun. **149**, 142 (2003) [arXiv:hep-ph/0201302].
9. W. Beenakker *et al.*, Phys. Rev. Lett. **87** (2001) 201805 [arXiv:hep-ph/0107081]; Nucl. Phys. B **653** (2003) 151 [arXiv:hep-ph/0211352]; S. Dawson *et al.*, Phys. Rev. D **67** (2003) 071503 [arXiv:hep-ph/0211438]; Phys. Rev. D **68** (2003) 034022 [arXiv:hep-ph/0305087].

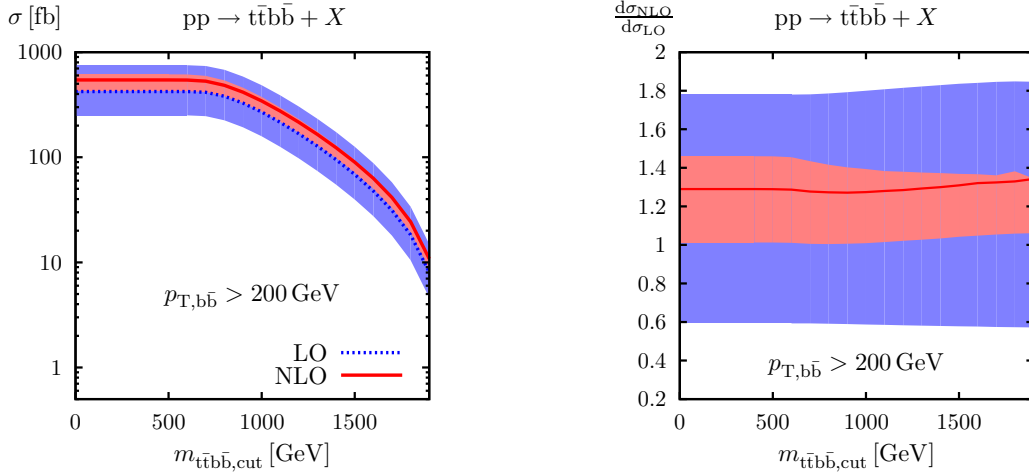


Figure 4. Dependence of the cross section with respect to a cut on the $t\bar{t}b\bar{b}$ invariant mass ($m_{t\bar{t}b\bar{b}} > m_{t\bar{t}b\bar{b},\text{cut}}$): absolute LO and NLO predictions (left) and NLO K factor (right).

10. G. Bevilacqua, M. Czakon, C. G. Papadopoulos and M. Worek, Phys. Rev. Lett. **104**, 162002 (2010) [arXiv:1002.4009 [hep-ph]].
11. R. Keith Ellis, K. Melnikov and G. Zanderighi, Phys. Rev. D **80**, 094002 (2009) [arXiv:0906.1445 [hep-ph]].
12. C. F. Berger *et al.*, Phys. Rev. D **80** (2009) 074036 [arXiv:0907.1984 [hep-ph]].
13. C. F. Berger *et al.*, arXiv:1004.1659 [hep-ph].
14. T. Binoth, *et al.*, Phys. Lett. B **685** (2010) 293 [arXiv:0910.4379 [hep-ph]].
15. A. Denner and S. Dittmaier, Nucl. Phys. B **658** (2003) 175 [arXiv:hep-ph/0212259]; Nucl. Phys. B **734** (2006) 62 [arXiv:hep-ph/0509141].
16. G. Ossola, C. G. Papadopoulos and R. Pittau, Nucl. Phys. B **763**, 147 (2007) [arXiv:hep-ph/0609007].
17. A. van Hameren, C. G. Papadopoulos and R. Pittau, JHEP **0909**, 106 (2009) [arXiv:0903.4665 [hep-ph]].
18. M. Czakon, C. G. Papadopoulos and M. Worek, JHEP **0908** (2009) 085 [arXiv:0905.0883 [hep-ph]].
19. J. Küblbeck, M. Böhm and A. Denner, Comput. Phys. Commun. **60** (1990) 165; H. Eck and J. Küblbeck, *Guide to FeynArts 1.0*, University of Würzburg, 1992.
20. T. Hahn, Comput. Phys. Commun. **140** (2001) 418 [arXiv:hep-ph/0012260].
21. T. Hahn and M. Pérez-Victoria, Comput. Phys. Commun. **118** (1999) 153 [arXiv:hep-ph/9807565]; T. Hahn, Nucl. Phys. Proc. Suppl. **89** (2000) 231 [arXiv:hep-ph/0005029].
22. G. 't Hooft and M. Veltman, Nucl. Phys. B **153** (1979) 365; W. Beenakker and A. Denner, Nucl. Phys. B **338** (1990) 349; A. Denner, U. Nierste and R. Scharf, Nucl. Phys. B **367** (1991) 637.
23. A. Denner and S. Dittmaier, arXiv:1005.2076 [hep-ph].
24. S. Dittmaier, Nucl. Phys. B **675** (2003) 447 [arXiv:hep-ph/0308246].
25. A. Denner, S. Dittmaier, M. Roth and L. H. Wieders, Nucl. Phys. B **724** (2005) 247 [arXiv:hep-ph/0505042].
26. S. Catani, S. Dittmaier, M. H. Seymour and Z. Trócsányi, Nucl. Phys. B **627** (2002) 189 [arXiv:hep-ph/0201036].
27. R. Frederix, T. Gehrmann and N. Greiner, JHEP **0809** (2008) 122 [arXiv:0808.2128 [hep-ph]].
28. J. Alwall *et al.*, JHEP **0709** (2007) 028 [arXiv:0706.2334 [hep-ph]].
29. J. Cammin and M. Schumacher, ATL-PHYS-

2003-024.